 doi:10.20944/preprints202107.0683.v1

Article

On the Static Pull-in of Tilting Actuation in Hybrid Levitation Micro-actuator: Theory and Experiment

Kirill Poletkin [1,2]

[1] Institute of Microstructure Technology - Karlsruhe Institute of Technology, Hermann-von-Helmholtz-Platz 1, 76344 Eggenstein-Leopoldshafen, Germany; kirill.poletkin@kit.edu
[2] Institute of Robotics and Computer Vision, Innopolis University, 1 Universitetskaya street, Innopolis City, 420500, Russian Federation; k.poletkin@innopolis.ru

Abstract: This work presents the results of the experimental and theoretical study of the static pull-in of tilting actuation executed by a hybrid levitation micro-actuator (HLMA) based on the combination of inductive levitation and electrostatic actuation. A semi-analytical model to study such the pull-in phenomenon is developed, for the first time, as a result of using the qualitative technique based on the Lagrangian approach to analyze inductive contactless suspensions presented in work [1] and a recent progress in the calculation of mutual inductance [2] and force [3] between two circular filaments. The obtained non-linear model, accounting for two degrees of freedom of the actuator, allows us to predict accurately the static pull-in displacement and voltage. The results of modelling were verified experimentally and agree well with measurements.

Keywords: micro-actuators; micro-systems; micro-manipulators; levitation; mutual inductance;

1. Introduction

Electromagnetic levitation micro-actuators employing remote ponderomotive forces, in order to act on a target environment or simply compensate a gravity force for holding stably a micro-object at the equilibrium without mechanical attachment, have already found wide applications and demonstrated a new generation of micro-sensors and -actuators with increased operational capabilities and overcoming the domination of friction over inertial forces at the micro-scale.

There are number of techniques, which provide the implementation of electromagnetic levitation into a micro-actuator system and can be classified according to the materials used and the sources of the force fields in two major branches: electric levitation micro-actuators (ELMA) and magnetic levitation micro-actuators (MLMA). In particular, ELMA were successfully used as linear transporters [4] and in micro-inertial sensors [5,6]. MLAM can be further split into inductive (ILMA), diamagnetic (DLMA), superconducting micro-actuators and hybrid levitation micro-actuators (HLMA) [7], which have found applications in micro-bearings [8–10], micro-mirrors [11,12], micro-gyroscopes [13,14], micro-accelerometers [15], bistable switches [16], nano-force sensors [17], micro-transporters [18], micro-accelerators [19], micro-motors [20–22] and resonators [23].

A wide spectrum of physical principles have been utilized and successfully implemented by using different techniques for micro-fabrication. However, recently developed 3D micro-coil technology [24] together with integration of a polymer magnetic composite material for flux concentration allows announcing inductive levitation micro-actuator systems, firstly, as systems with established micro-fabrication process in comparison to the other levitation actuator systems and, secondly, as high-performance systems. As a results of this progress, our group demonstrated the inductive levitation actuator system with the record lowest current consumption [10] around tens of mA. This permits us to avoid using standard bulky high frequency current amplifiers for exciting the ILMA and to replace them by the integrated control circuit including the signal generator and amplifier and having a size comparable with size of micro-actuator system [25].

Preprints (www.preprints.org) | NOT PEER-REVIEWED | Posted: 30 July 2021 doi:10.20944/preprints202107.0683.v1

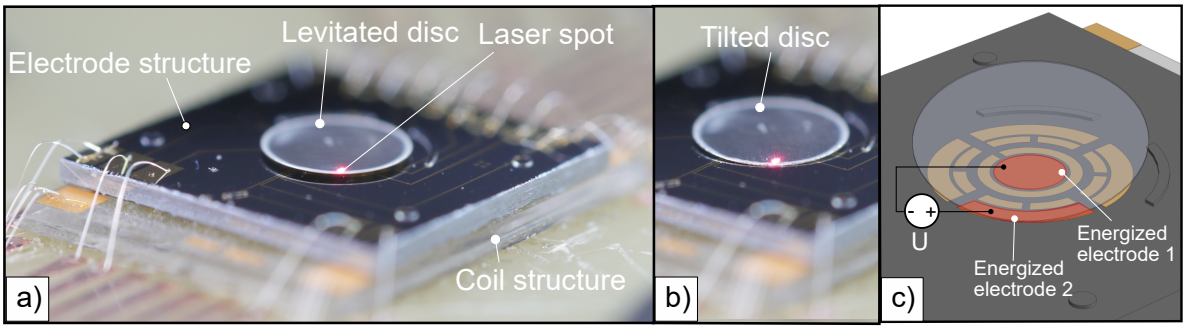

Figure 1. Experimental test of tilting actuation in hybrid levitation micro-actuator and scheme of electrode set: a) stable levitation of the disc having a diameter of 2.8 mm; b) applying the pull-in voltage to the electrodes, the disc was tilted. The angle of tilting actuation is restricted by the mechanical contact with the surface of the electrode structure: c) the set of electrodes (the energized electrodes are highlighted in red, U is the applied voltage).

HLMAs, in which for instance the inductive levitation micro-actuator system can be joined with a source of electrostatic field, dramatically increase capabilities of levitated micro-systems [26] and demonstrate a wide range of different operation modes such as the linear and angular positioning, bi-stable linear and angular actuation and the adjustment of stiffness components as it was reported in [20,27] and presented by the author at Transducers 2017 [28]. These capabilities open a new very promising perspective to create smart micro-actuator systems with new functional abilities implemented, for instance, by means of the coherent cooperation of distributed microactuators, multi-stable actuation, mechanical and electromagnetic couplings.

Although, the linear pull-in actuation has been comprehensively studied theoretically as well as experimentally [29], however angular pull-in phenomenon of tilting actuation in such HLMAs has not yet been addressed. In this article, in order to fill this gap, a prototype of hybrid levitation micro-actuator was fabricated to experimentally demonstrate and characterise the static pull-in behaviour of tilting actuation. Using the qualitative technique based on the Lagrangian approach [1], a semi-analytical model for mimicking such the static pull-in behaviour based on two circuit approximation of induced eddy current with proof mass is developed. Upon tilting the levitated disc, the geometrical transformation of eddy current circuit is analysed by means of finite element approach proposed in [30]. As a result of this analysis becomes a semi-analytical function for calculation mutual inductance and corresponding electromagnetic force and torque developed by Kalantarov-Zeitlin's method [2]. Thus, the particularity of the developed model is to employ this new derived function for calculation mutual inductance and to account for two degrees of freedom, namely, linear displacement in the vertical direction and angular one of the levitated disc. Through this study we verified successfully the given assumptions for modelling and developed the robust analytical tool to describe the static pull-in actuation of HLMAs.

2. Fabrication and measurements

In order to comprehensively study the static pull-in of tilting actuation executed by the HLMA, we fabricated a micro-prototype as shown Fig. 1a) by using a similar fabrication process reported in work [20]. Namely, the hybrid actuator consists of two structures fabricated independently, namely, the coil structure and the electrode structure, which were aligned and assembled by flip-chip bonding into one device with the dimensions: 9.4 mm×7.4 mm×1.1 mm as shown in Fig. 1a).

The coil structure includes two coaxial 3D wire bonded microcoils similar to those reported in our previous work [9], namely the stabilization and the levitation coils, fabricated on Pyrex substrate using SU-8 2150. The function of the coil structure is to stably levitate an aluminium disc-shaped proof mass (PM). For this particular device, the height of the coils is 500 µm and the number of windings is 20 and

12 for levitation and stabilization coils, respectively. This coil structure is able to levitate PMs with diameters ranging from 2.7 to 3.3 mm [9].

The top electrode structure was fabricated on a SOI wafer having a device layer of 40 µm, the buried oxide of 2 µm, a handle layer of 600 µm and the resistivity of silicon in a range of 1..30 Ω cm as it was reported in work [31]. Also, the device layer has a 500 nm oxide layer for passivation, on the top of which electrodes are patterned by UV lithography on evaporated Cr/Au layers (20/150 nm). The design of electrode set is schematically shown in Fig. 1c). After etching the handle layer up to the buried oxide by DRIE, the bottom electrode structure was aligned and bonded onto the coil structure. Finally, the fabricated device was glued on a PCB board as shown in Fig. 1a).

The actuator coils were feeded by ac current at the frequency of 10 MHz, with a rms value ranging from 100 mA to 130 mA. This range of changing of ac current allowed us to levitating a disc having a diameter of 2.8 mm within a height from 35 to 190 µm measured from the surface of the electrodes patterned on the silicon substrate. Pull-in of tilting actuation was performed by applying pull-in voltage to electrode "1" and "2" as shown in Fig. 1b) and c). The circular electrode "1" has a diameter of 1 mm corresponding to an area of around $\sim$0.8 mm^2. While, the geometry of the sectorial electrode "2" is characterised by the following parameters: an inner radius of 1.1 mm, an outer radius of 1.4 mm and the center angle of $\pi/2$ rad, which is corresponding to an area of around $\sim$0.43 mm^2. The electrode set was able to generate the tilting torque within a range of 0.7×10^{-10} N m. The linear displacement of a disc edge was measured by a laser distance sensor directly (see, Fig. 1a), b)). The measurements were performed at two levitation heights. Namely, the disc was levitated at 130 and 150 µm. The pull-in actuation occurred for the applied voltage of 27 and 33 V and the measured pull-in displacements were 34 and 45 µm, respectively. The results of measurements accompanying with results of modeling are summed up in Table 1 below.

3. Simulation and modeling

The mechanism of stable levitation of the disc shaped proof mass in the framework of two coil design is as follows. The induced eddy currents are distributed along the levitated proof mass in such a way that two circuits having maximum values of eddy current density can be identified. The first circuit corresponds to the eddy current distributed along the edge of disc-shaped PM and the second circuit is defined by the levitation coil. The later one has a circular path with radius equal to the radius of the levitation coil. Hence, this mechanism can be split into two force interactions. The force interaction happens between the current in the stabilization coil and induced eddy current corresponding to the first circuit, which contributes mainly to the lateral stability of the levitated PM. While, the force interaction between the current in the levitation coil and induced eddy current related to the second circuit contributes mainly to the vertical and angular stability of the levitated PM [1].

Upon tilting the PM, the eddy current circuit generated by the levitation coil is transformed form a circular shape into elliptical one. In the section below, this transformation of the shape of eddy current circuit is analyzed by quasi-finite element approach recently developed in [30,32,33]. As a result of the analysis, formulas for calculation of the mutual inductance and corresponding electromagnetic torque and force acting on the PM are derived by employing Kalantarov-Zeitlin's method [2]. Then the derived formulas are applied for the modeling of the pull-in actuation in the HLMA.

3.1. Simulation of induced eddy current within the tilting proof mass

According to the procedure proposed in our previous work [30], the disc is meshed by circular elements as it is shown in Fig. 2a). For the particular case, the levitated micro-disc is meshed by circular elements each of them has the same radius of R_e =2.4814 $\times 10^{-5}$ m. For the disc of a diameter of 2.8mm, a number of elements is $n = 2496$. 3D scheme of two micro-coils is approximated by a series of circular filaments. The levitation coil is replaced by 20 circular filaments having a diameter of 2.0 mm, while the stabilization coil by 12 circular filaments with a diameter of 3.8 mm. Thus, the total number of circular filaments, N, is 32. Assigning the origin of the fixed frame $\{X_k\}$ $(k = 1, 2, 3)$

Preprints (www.preprints.org) | NOT PEER-REVIEWED | Posted: 30 July 2021 doi:10.20944/preprints202107.0683.v1

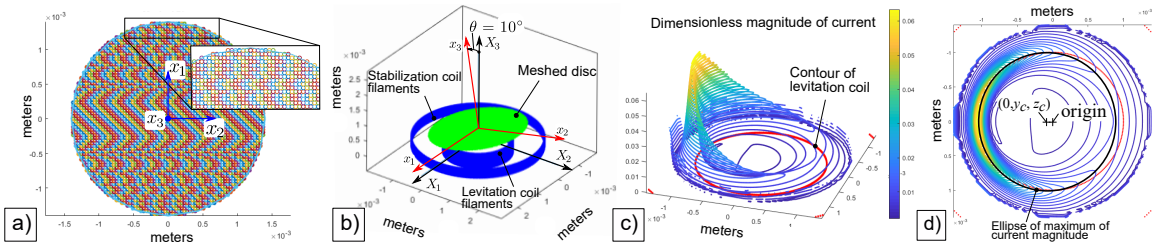

Figure 2. 3D geometrical scheme of the actuator for simulation mimicking the real prototype of actuator shown on the right side of the figure: $\{X_k\}$ $(k = 1, 2, 3)$ is the fixed coordinate frame.

to the centre of the circular filament corresponding to the first top winding of the levitation coil, the linear position of the circular filaments of levitation coil can be defined as ${}^{(j)}r_c = [0\ 0\ (j-1)\cdot p]^T$, $(j = 1, \ldots, 20)$, where p is the pitch equaling to 25 µm. The same is applicable for stabilization coil, ${}^{(j)}r_c = [0\ 0\ (j-21)\cdot p]^T$, with the difference that the index j is varied from 21 to 32. For both coils, the Brayn angle of each circular filament is ${}^{(j)}\underline{\phi}_c = [0\ 0\ 0]^T$, $(j = 1, \ldots, 32)$.

The result of meshing becomes a list of elements $\{{}^{(s)}\underline{C} = [{}^{(s)}\rho\ {}^{(s)}\phi]^T\}$ $(s = 1, \ldots, n)$ containing information about a radius vector and an angular orientation for each element with respect to the coordinate frame $\{x_k\}$ $(k = 1, 2, 3)$. Now a matrix $\underline{L}$ of self-inductances of circular elements and mutual inductances between them can be formed as follows

$$\underline{L} = L^o\underline{E} + \underline{M}^o, \tag{1}$$

where $\underline{E}$ is the (2496×2496) unit matrix, $\underline{M}^o$ is the (2496×2496) -symmetric hollow matrix whose elements are L^o_{ks} $(k \neq s)$. The self-inductance of the circular element is calculated by the known formula for a circular ring of circular cross-section

$$L^o = \mu_0 R_e \left[\ln 8/\varepsilon_t - 7/4 + \varepsilon_t^2/8\,(\ln 8/\varepsilon_t + 1/3)\right], \tag{2}$$

where μ_0 is the magnetic permeability of free space, $\varepsilon_t = th/(2R_e)$, th is the thickness of a meshed layer of micro-object (in the particular case, th =13 µm).

Accounting for the values of diameters of levitation and stabilization coils, 3D geometrical scheme of the actuator for the eddy current simulation can be build as shown in Fig. 2b). The position of the coordinate frame $\{x_k\}$ $(k = 1, 2, 3)$ with respect to the fixed frame $\{X_k\}$ $(k = 1, 2, 3)$ is defined by the radius vector $\boldsymbol{r}_{cm} = [0\ 0\ h_l]^T$, where the levitation height, h_l is to be 100 µm. Then, the position of the s-mesh element with respect to the coordinate frame $\{{}^{(j)}z_k\}$ $(k = 1, 2, 3)$ assigned to the j-coil filament can be found as ${}^{(s,j)}\boldsymbol{r} = \boldsymbol{r}_{cm} + {}^{(s)}\boldsymbol{\rho} - {}^{(j)}\boldsymbol{r}_c$ or in a matrix form as

$${}^{(s,j)}\underline{r}^z = {}^{(j)}\underline{A}^{zX}\underline{r}^X_{cm} + {}^{(j)}\underline{A}^{zx}{}^{(s)}\underline{\rho}^x - {}^{(j)}\underline{A}^{zX}{}^{(j)}\underline{r}^X_c, \tag{3}$$

where ${}^{(j)}\underline{A}^{zX} = {}^{(j)}\underline{A}^{zX}\left({}^{(j)}\underline{\phi}_c\right) = {}^{(j)}\underline{e}^z \cdot \underline{e}^X$ and ${}^{(j)}\underline{A}^{zx} = {}^{(j)}\underline{A}^{zX}\left({}^{(j)}\underline{\phi}_c\right)\underline{A}^{Xx}(\underline{\varphi}) = {}^{(j)}\underline{e}^z \cdot \underline{e}^x$ are the direction cosine matrices, $\underline{\varphi} = [\theta\ 0\ 0]$ is the vector of the angular generalized coordinates.

Since all matrices of ${}^{(j)}\underline{\phi}_c$ are zeros. Hence, ${}^{(j)}\underline{A}^{zX} = \underline{E}$, where $\underline{E}$ is the (3×3) unit matrix and ${}^{(j)}\underline{A}^{zx} = {}^{(j)}\underline{A}^{zX}\left({}^{(j)}\underline{\phi}_c\right)\underline{A}^{Xx}(\underline{\varphi}) = \underline{E}\,\underline{A}^{Xx}(\underline{\varphi}) = \underline{A}^{Xx}(\underline{\varphi})$. As an illustrative example, the angle θ is chosen to be 10° as shown in Fig. 2b). Moreover, the coils are represented by the circular filaments and using the radius vector ${}^{(s,j)}\boldsymbol{r}$, the mutual inductance between the j- coil and s-meshed element can be calculated directly by the formula presented in [2]. Thereby, the the (2496×32) matrix $\underline{M}_c$ of mutual inductance between coils and finite elements can be formed. The induced eddy current in each circular element is a solution of the following matrix equation

$$\underline{I} = \underline{L}^{-1}\underline{M}_c\underline{I}_c, \tag{4}$$

Preprints (www.preprints.org) | NOT PEER-REVIEWED | Posted: 30 July 2021 doi:10.20944/preprints202107.0683.v1

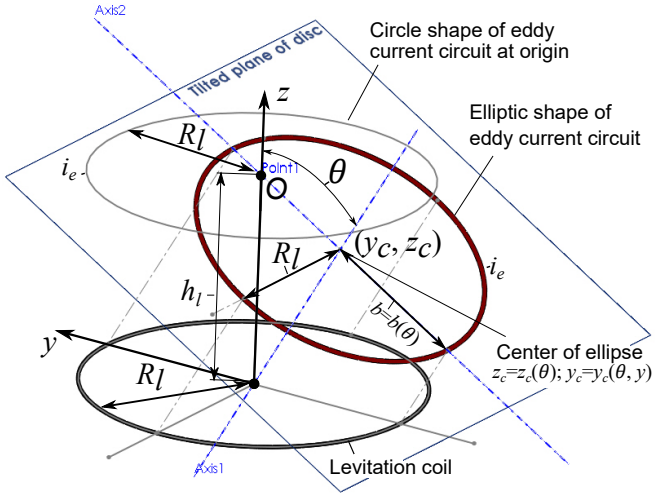

Figure 3. Reduced scheme for modelling electromagnetic interaction between the levitation coil and the tilt-disc: h_l is the levitation height between a plane of coils and equilibrium point; θ is the tilting angle; i_e is the induced eddy current corresponding to the maximum current density within the disc; R_l is the radius of the levitation coil; $z_c = z_c(\theta)$ and $y_c = y_c(\theta, z_c)$ are the coordinates of the center of the ellipse as functions of generalized coordinates; $b = b(\theta)$ is the length of minor axis of the ellipse.

where $\underline{I}$ is the (2496×1) matrix of eddy currents and $\underline{I}_c = [I_{c1} I_{c2} \dots I_{cN}]^T$ is the given (32×1) matrix of currents in coils.

For calculation, dimensionless currents in the levitation coil and stabilization one are introduced by dividing currents on the amplitude of the current in the levitation coil. Noting that the amplitude of the current in both coils are the same. Hence, the input current in the levitation coil filaments is to be one, while in the stabilization coil filaments to be minus one (because of the 180° phase shift). Now, the induced eddy current in dimensionless values can be calculated [30]. The result of calculation is shown in Fig. 2c) as a 3D plot. The intensity of the color shown by the bar characterizes the value of dimensionless magnitude of the eddy current. Fig. 2d) shows a 2D plot of the distribution of magnitudes of eddy current along the area of the surface of the PM. As it is seen from Figures 2c) and d) that the maximum of eddy current magnitudes are distributed along the edge of the PM and around its centre. Besides, the analysis of Fig. 2d) depicts that a circular shape of maximum magnitude of eddy current induced by the current of the stabilization coil without tilting the PM [30] is transformed into an elliptical shape with shifting its centre as shown in Fig. 2d). The centre of the ellipse is characterized by the following coordinates $z_c = z_c(\theta)$ and $y_c = y_c(\theta)$, which are also functions of the tilting angle θ.

3.2. Mutual Inductance between two filaments of circular and elliptic shapes

Approximating the elliptical shape of distribution of the eddy current magnitude around the centre of the PM by a filament, a function for calculation of the mutual inductance between the elliptical filament with the shifted centre and circular filament is derived by using Kalantarov-Zeitlin's method. Scheme with detailed particularities of geometry for calculation is shown in Fig. 3.

Accounting for Fig. 3 and introducing the following dimensionless coordinates:

$$z = \frac{z_c}{R_l};\ y = -z\frac{\tan(\theta)}{\tan^2(\theta)+1}, \tag{5}$$

the formula for calculation of the mutual inductance can be written as

$$M = \frac{\mu_0 R_l}{\pi}\int_0^{2\pi} r \cdot F \cdot \Phi(k) d\varphi, \tag{6}$$

Preprints (www.preprints.org) | NOT PEER-REVIEWED | Posted: 30 July 2021 doi:10.20944/preprints202107.0683.v1

where

$$r = r(\theta) = \frac{\cos\theta}{\sqrt{(\tan^2(\theta)+1)\sin^2(\varphi)+\cos^2(\theta)\cos^2(\varphi)}}, \tag{7}$$

$$F = F(\theta, z) = \frac{R}{\rho^{1.5}} = \frac{r + t_1 \cdot \cos\varphi + t_2 \cdot \sin\varphi}{\rho^{1.5}}, \tag{8}$$

$$\begin{aligned} &\rho^2 = \rho^2(\theta, z) = r^2 + 2r \cdot y \sin(\varphi) + y^2, \\ &t_1 = t_1(\theta, z) = 0.5 \cdot r^2 \tan^2\theta \sin(2(\varphi)) \cdot y,\ t_2 = t_2(\theta, z) = y, \end{aligned} \tag{9}$$

$$\Phi(k) = \frac{1}{k}\left[\left(1 - \frac{k^2}{2}\right)K(k) - E(k)\right], \tag{10}$$

and $K(k)$ and $E(k)$ are the complete elliptic functions of the first and second kind, respectively, and

$$\begin{aligned} &k^2 = k^2(\theta, z) = \frac{4\rho}{(\rho+1)^2 + z_\lambda^2}, \\ &z_\lambda = \frac{z}{\tan^2(\theta)+1} + r\tan\theta\sin(\varphi). \end{aligned} \tag{11}$$

3.3. Model of static pull-in of tilting actuation

Assuming that the contribution of the force interaction between the current in the stabilization coil and the eddy current circuit flowing along the edge of the PM to the behaviour of the PM in the vertical and angular directions measured by the generalized coordinates z_c and θ, respectively, is negligible [30]. Thus, the force interaction between the current in the levitation coil and the eddy current distributed around PM's centre is dominated and determines the actuation of the PM under applying electrostatic force produced by the energized electrodes "1" and "2".

Hence, the Lagrangian of the electromagnetic system under consideration can be written as

$$L = \frac{1}{2}m\dot{z}_c^2 + \frac{1}{2}J\dot{\theta}^2 - mgz_c + M(\theta, z_c)Ii + \frac{1}{2}L_e(\theta, z_c)i^2 - \frac{1}{2}\frac{Q_1^2}{C_1(\theta, z_c)} - \frac{1}{2}\frac{Q_2^2}{C_2(\theta, z_c)}, \tag{12}$$

where m is the mass of PM, J is the moment of inertia of the disc about axis through centre of mass and coinciding with its diameter, g is the gravitational acceleration, $M(\theta, z_c)$ is the mutual inductance defined by formula (6), I is the given ac current in the levitation coil ($I = \hat{I}e^{j\omega t}$, where $\hat{I}$ is the magnitude, ω is the frequency), i is the induced eddy current, L_e is the self inductance of the eddy current circuit, Q_1 and Q_2 are the charges stored by the planar capacitors C_1 and C_2 build on electrodes "1" and "2", respectively. Accounting for linear and angular displacements of the PM, the capacitances corresponding to circular "1" and sectorial "2" electrode can be described, respectively, by the following equations

$$\begin{aligned} &C_1(\theta, z_c) = -\varphi_{10}\frac{h_l + z_c}{\tan^2(\theta)}\ln\left(1 - \frac{R_1^2\tan^2(\theta)}{(h_l + z_c)^2}\right); \\ &C_2(\theta, z_c) = \frac{\varphi_{20}}{\tan(\theta)}\left[R_{out} - R_{in} + \frac{h_l + z_c}{\tan(\theta)}\ln\left(\frac{1 + R_{in}\tan(\theta)/(h_l + z_c)}{1 + R_{out}\tan(\theta)/(h_l + z_c)}\right)\right], \end{aligned} \tag{13}$$

where $\varphi_{10} = \pi\varepsilon\varepsilon_0$ and $\varphi_{20} = \varepsilon\varepsilon_0\pi/2$, ε is the relative permittivity and ε_0 is the permittivity of free space, R_1 is the radius of the centre electrode, R_{out} and R_{in} are the outer and inner radii of the sectorial electrode, respectively. Noting that the capacitors are connected in the series, due to this fact for charges we can write that $Q_1 = Q_2 = Q$. The dissipation function can be presented as

$$\Psi = \frac{1}{2}R_e i^2, \tag{14}$$

Preprints (www.preprints.org) | NOT PEER-REVIEWED | Posted: 30 July 2021 doi:10.20944/preprints202107.0683.v1

where R_e is the electrical resistance of the eddy current circuit. Hence, the state of the system can be defined by two coordinates z_c and θ, the charge Q and the eddy current i.

Adapting the variables and the assumptions introduced above, the Lagrange - Maxwell equations of the system can be written as follows

$$\begin{cases} \dfrac{d}{dt}\left(\dfrac{\partial L}{\partial i}\right) + \dfrac{\partial \Psi}{\partial i} = 0; & -\dfrac{\partial L}{\partial Q} = U; \\ \dfrac{d}{dt}\left(\dfrac{\partial L}{\partial \dot{z}_c}\right) - \dfrac{\partial L}{\partial z_c} = 0; & \dfrac{d}{dt}\left(\dfrac{\partial L}{\partial \dot{\theta}}\right) - \dfrac{\partial L}{\partial \theta} = 0. \end{cases} \tag{15}$$

Substituting (12) and (14) into (15) and accounting for the fact that the static problem is considered, so the acceleration and speed of coordinates z_c and θ are ignored. Thus, we can finally write the following set of equations describing the static behaviour of the PM [1]:

$$\begin{cases} L_e \dfrac{di}{dt} + R_e i + M\dfrac{dI}{dt} = 0; & \dfrac{C_2 + C_1}{C_1 C_2} Q = U; \\ mg - \dfrac{\partial M}{\partial z_c} Ii - \dfrac{1}{C_1 + C_2}\left(C_2^2 \dfrac{\partial C_1}{\partial z_c} + C_1^2 \dfrac{\partial C_2}{\partial z_c}\right) U^2 = 0; \\ -\dfrac{\partial M}{\partial \theta} Ii - \dfrac{1}{C_1 + C_2}\left(C_2^2 \dfrac{\partial C_1}{\partial \theta} + C_1^2 \dfrac{\partial C_2}{\partial \theta}\right) U^2 = 0. \end{cases} \tag{16}$$

Since the system operated in the air and the air damping supports the stable levitation of the PM, hence we can conclude similar to [1] that $i \approx -MI$. Substituting the relation for currents from the later conclusion into (16) and averaging ponderomotive force and torque with respect to the time ($1/2\pi \int_0^{2\pi} \frac{\partial M}{\partial g} \Re(i)\Re(I)dt = 1/2\hat{I}^2$, where $g = \theta,\ z_c$), we can write

$$\begin{cases} mg - \dfrac{1}{2}\dfrac{\partial M}{\partial z_c} M\hat{I}^2 - \dfrac{1}{C_1 + C_2}\left(C_2^2 \dfrac{\partial C_1}{\partial z_c} + C_1^2 \dfrac{\partial C_2}{\partial z_c}\right) U^2 = 0; \\ -\dfrac{1}{2}\dfrac{\partial M}{\partial \theta} M\hat{I}^2 - \dfrac{1}{C_1 + C_2}\left(C_2^2 \dfrac{\partial C_1}{\partial \theta} + C_1^2 \dfrac{\partial C_2}{\partial \theta}\right) U^2 = 0. \end{cases} \tag{17}$$

4. Analysis of the derived model

The semi-analytical model (17) to describe the static pull-in actuation of the fabricated prototype is developed by employing the qualitative technique to analyze inductive contactless suspensions, and new formula for calculation of mutual inductance between the circular filament and its projection on a tilted plane derived in Sec. 3.2 based on the result of simulation of induced eddy current within disc shaped PM obtained by means of quasi-FEM approach. The mechanical behavior of the disc is described by two generalized coordinates. They can be represented by dimensionless variables, namely $\overline{\theta} = R_T\theta/h$ is the dimensionless angle and $\lambda = z_c/h$ is the dimensionless displacement, where h is

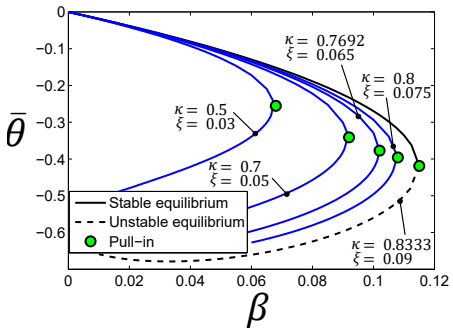

Figure 4. Stable and unstable angular equilibrium of the tilt-disc and its evolution depending on the parameters of device such as $\xi = h_l/2R_l$ and $\kappa = h/h_l$, where h is the space between an electrodes plane and equilibrium point of the disc, R_l is the radius of levitation coil.

Preprints (www.preprints.org) | NOT PEER-REVIEWED | Posted: 30 July 2021 doi:10.20944/preprints202107.0683.v1

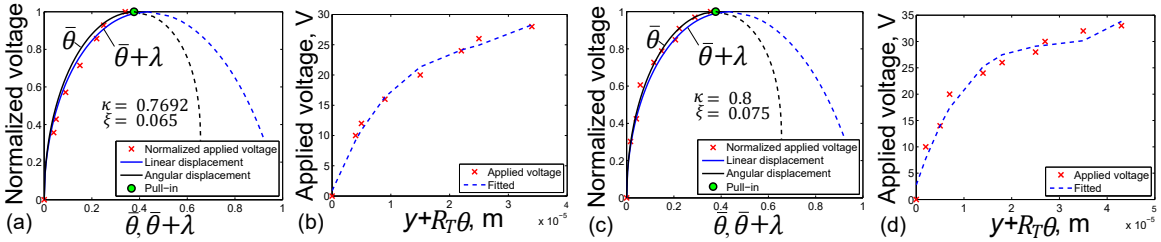

Figure 5. Static pull-in of tilting actuation: a) comparison of modelling with results of measurement I; b) applied voltage vs the linear displacement of the disc for measurement I; c) comparison of modelling with results of measurement II; b) applied voltage vs the linear displacement of the disc for measurement II (other details are shown in Table 1).

the spacing between the surface electrode structure and an equilibrium point O; $R_T = (R_{out} + R_{in})/2$ is the distance between the centre of the disc and applied electrostatic force generated by electrode "2". The electromagnetic part of this system is reduced to the interaction between the current in the levitation coil and the induced eddy current with circuit corresponding to its maximum density within the disc. As a result of numerical analysis, the behavior of the shape of induced maximum density of eddy current within the disc was represented via an analytical function of introduced above two generalized coordinates. This circumstance helps us to exactly define the mutual inductance and then to calculate the magnetic force and torque acting on the disc.

A preliminary result of modelling are shown in Fig. 4, which provides an evolution of bifurcation diagrams for equilibrium of the titling PM without linear displacement depending on the applied dimensionless voltage $\sqrt{\beta} = \sqrt{\varepsilon_0 A_1 U^2/(2mgh^2(1+a))}$, where A_1 and A_2 are the areas of electrode 1 and 2, respectively, $a = A_1/A_2$ and depending on dimensionless parameters characterizing geometrical particularities of the prototype design, namely, $\kappa = h/h_l$, which is in a range from 0.5 to 0.9, and $\xi = h_l/(2R_l)$, which is changing in a range from 0.03 to 0.09. These ranges of parameters κ and ξ are typical for all known designs of HLMA studied in the literature. As it is seen from Fig. 4, increasing a radius of levitation coil (it means that ξ is respectively decreased) and decreasing the space h (it means that the dimensionless parameter κ is also decreased) leads to decreasing pull-in voltage and displacement.

Modelling the experimental measurement discussed in Sec. 2 requires taking into account the angular as well as linear displacement of the disc due to essential contribution of linear force acting along the z axis. Fig. 5 shows the comparison of results of measurements and modelling in normalized values. As a result of the contribution of the linear force, the range of angular displacement is reduced by 40%.

Fig. 6 reveals the direct comparison between measurements and modelling. The parameters of the device, particularities of conducted measurements and obtained results are summed up in Table 1. The analysis of Fig. 5, 6 and Table 1 shows that the modelling agrees well with experimental data.

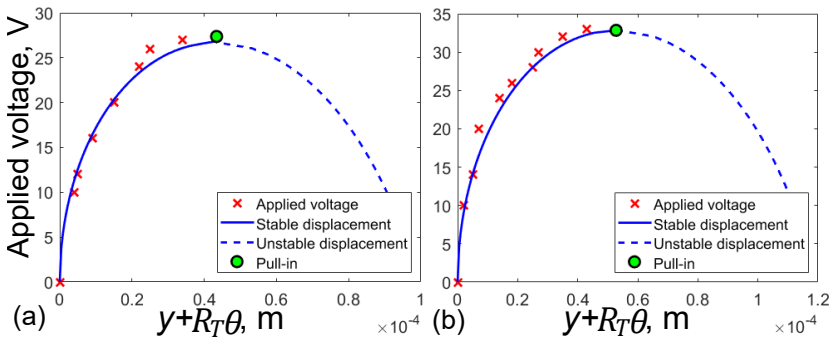

Figure 6. Direct comparison of results of measurements and modelling (displacements are shown in absolute values): a) for measurement I ; b) for measurement II (other details are shown in Table 1).

Preprints (www.preprints.org) | NOT PEER-REVIEWED | Posted: 30 July 2021 doi:10.20944/preprints202107.0683.v1

Table 1. Results of measurements and modelling of the static pull-in.

	Parameters	Measurement I	Measurement II
Measured	Levitation height, h_l	130 µm	150 µm
	Spacing, h	100 µm	120 µm
	Pull-in displacement	**34** µm	**45** µm
	Pull-in voltage, U	**27** V	**33** V
Modelled	$\xi = h_l/2R_l$	0.065	0.075
	$\kappa = h/h_l$	0.7692	0.8
	Pull-in displacement	**38** µm	**48** µm
	Pull-in voltage, U	**28** V	**33** V
Device	Diameter of levitation coil, d_l	2 mm	
	Area of electrodes, A_1 and A_2	0.8 and 0.43 mm^2	

5. Conclusions

In this article, the static pull-in of tilting actuation in HLMA was studied theoretically as well as experimentally. The semi-analytical model (17) mimicking the static pull-in behaviour of tilting actuation in HLMA is developed by employing the qualitative technique to analyze the dynamics and stability of inductive contactless suspensions, and new formula for calculation of mutual inductance between the circular filament and its projection on a tilted plane. As the result of simulation of induced eddy current within disc shaped PM carried out quasi-FEM approach, which showed the distribution of eddy current around the centre of a conducting disc, this new formula was developed and presented in the integral form based on Kalantarove-Zeitlin's method. The obtained non-linear model, accounting for two degrees of freedom of the actuator, allows us to predict accurately the static pull-in displacement and voltage for the particular prototype of HLMA. The results of modelling were verified experimentally and agree well with measurements. Through this study we verified successfully the given assumptions for modelling and developed the robust analytical tool to describe the static pull-in actuation and to predict pull-in parameters for HLMAs.

Funding: This research was funded by the German Research Foundation grant number KO 1883/37-1 within the priority program SPP2206 "KOMMMA", project "A 2D array of cooperative hybrid levitation micro- actuators".

Conflicts of Interest: The author declares no conflict of interest.

Abbreviations

The following abbreviations are used in this manuscript:

ILMA	Inductive Levitation Micro-Actuator
HLMA	Hybrid Levitation Micro-Actuator
PM	Proof Mass
MLMA	Magnetic Levitation Micro-Actuator
ELMA	Electric Levitation Micro-Actuator

References

1. Poletkin, K.; Lu, Z.; Wallrabe, U.; Korvink, J.; Badilita, V. Stable dynamics of micro-machined inductive contactless suspensions. *International Journal of Mechanical Sciences* **2017**, *131-132*, 753 – 766. doi:https://doi.org/10.1016/j.ijmecsci.2017.08.016.
2. Poletkin, K.V.; Korvink, J.G. Efficient calculation of the mutual inductance of arbitrarily oriented circular filaments via a generalisation of the Kalantarov-Zeitlin method. *Journal of Magnetism and Magnetic Materials* **2019**, *483*, 10–20. doi:https://doi.org/10.1016/j.jmmm.2019.03.078.
3. Poletkin, K. Calculation of force and torque between two arbitrarily oriented circular filaments using Kalantarov-Zeitlin's method. *arXiv preprint arXiv:2106.09496* **2021**.

4. Jin, J.; Yih, T.C.; Higuchi, T.; Jeon, J.U. Direct electrostatic levitation and propulsion of silicon wafer. *IEEE Transactions on Industry Applications* **1998**, *34*, 975–984. doi:10.1109/28.720437.
5. Murakoshi, T.; Endo, Y.; Fukatsu, K.; Nakamura, S.; Esashi, M. Electrostatically levitated ring-shaped rotational gyro/accelerometer. *Jpn. J. Appl. Phys* **2003**, *42*, 2468–2472.
6. Han, F.T.; Liu, Y.F.; Wang, L.; Ma, G.Y. Micromachined electrostatically suspended gyroscope with a spinning ring-shaped rotor. *Journal of Micromechanics and Microengineering* **2012**, *22*, 105032.
7. Poletkin, K.V.; Asadollahbaik, A.; Kampmann, R.; Korvink, J.G. Levitating Micro-Actuators: A Review. *Actuators* **2018**, *7*. doi:10.3390/act7020017.
8. Coombs, T.A.; Samad, I.; Ruiz-Alonso, D.; Tadinada, K. Superconducting micro-bearings. *IEEE Transactions on Applied Superconductivity* **2005**, *15*, 2312–2315. doi:10.1109/TASC.2005.849640.
9. Lu, Z.; Poletkin, K.; den Hartogh, B.; Wallrabe, U.; Badilita, V. 3D micro-machined inductive contactless suspension: Testing and modeling. *Sensors and Actuators A: Physical* **2014**, *220*, 134 – 143. doi:https://doi.org/10.1016/j.sna.2014.09.017.
10. Poletkin, K.V.; Lu, Z.; Moazenzadeh, A.; Mariappan, S.G.; Korvink, J.G.; Wallrabe, U.; Badilita, V. Polymer Magnetic Composite Core Boosts Performance of Three-Dimensional Micromachined Inductive Contactless Suspension. *IEEE Magnetics Letters* **2016**, *7*, 1–3. doi:10.1109/LMAG.2016.2612181.
11. Shearwood, C.; Williams, C.B.; Mellor, P.H.; Chang, K.Y.; Woodhead, J. Electro-magnetically levitated micro-discs. IEE Colloquium on Microengineering Applications in Optoelectronics, 1996, pp. 6/1–6/3. doi:10.1049/ic:19960241.
12. Xiao, Q.; Wang, Y.; Dricot, S.; Kraft, M. Design and experiment of an electromagnetic levitation system for a micro mirror. *Microsystem Technologies* **2019**, *25*, 3119–3128.
13. Shearwood, C.; Ho, K.Y.; Williams, C.B.; Gong, H. Development of a levitated micromotor for application as a gyroscope. *Sensor. Actuat. A-Phys.* **2000**, *83*, 85–92.
14. Su, Y.; Xiao, Z.; Ye, Z.; Takahata, K. Micromachined Graphite Rotor Based on Diamagnetic Levitation. *IEEE Electron Device Letters* **2015**, *36*, 393–395. doi:10.1109/LED.2015.2399493.
15. Garmire, D.; Choo, H.; Kant, R.; Govindjee, S.; Sequin, C.; Muller, R.; Demmel, J. Diamagnetically levitated MEMS accelerometers. Solid-State Sensors, Actuators and Microsystems Conference, 2007. TRANSDUCERS 2007. International. IEEE, 2007, pp. 1203–1206.
16. Dieppedale, C.; Desloges, B.; Rostaing, H.; Delamare, J.; Cugat, O.; Meunier-Carus, J. Magnetic bistable micro-actuator with integrated permanent magnets. Proc. IEEE Sensors, 2004, Vol. 1, pp. 493–496.
17. Abadie, J.; Piat, E.; Oster, S.; Boukallel, M. Modeling and experimentation of a passive low frequency nanoforce sensor based on diamagnetic levitation. *Sensor. Actuat. A-Phys.* **2012**, *173*, 227–237.
18. Poletkin, K.V.; Lu, Z.; Wallrabe, U.; Korvink, J.G.; Badilita, V. A qualitative technique to study stability and dynamics of micro-machined inductive contactless suspensions. 2017 19th International Conference on Solid-State Sensors, Actuators and Microsystems (TRANSDUCERS), 2017, pp. 528–531. doi:10.1109/TRANSDUCERS.2017.7994102.
19. Sari, I.; Kraft, M. A MEMS Linear Accelerator for Levitated Micro-objects. *Sensor. Actuat. A-Phys.* **2015**, *222*, 15–23.
20. Poletkin, K.; Lu, Z.; Wallrabe, U.; Badilita, V. A New Hybrid Micromachined Contactless Suspension With Linear and Angular Positioning and Adjustable Dynamics. *Journal of Microelectromechanical Systems* **2015**, *24*, 1248–1250. doi:10.1109/JMEMS.2015.2469211.
21. Xu, Y.; Cui, Q.; Kan, R.; Bleuler, H.; Zhou, J. Realization of a Diamagnetically Levitating Rotor Driven by Electrostatic Field. *IEEE/ASME Transactions on Mechatronics* **2017**, *22*, 2387–2391. doi:10.1109/TMECH.2017.2718102.
22. Xu, Y.; Zhou, J.; Bleuler, H.; Kan, R. Passive diamagnetic contactless suspension rotor with electrostatic glass motor. *Micro & Nano Letters* **2019**, *14*, 1056–1059.
23. Chen, X.; Keskekler, A.; Alijani, F.; Steeneken, P.G. Rigid body dynamics of diamagnetically levitating graphite resonators. *Applied Physics Letters* **2020**, *116*, 243505, [https://doi.org/10.1063/5.0009604]. doi:10.1063/5.0009604.
24. Kratt, K.; Badilita, V.; Burger, T.; Korvink, J.; Wallrabe, U. A fully MEMS-compatible process for 3D high aspect ratio micro coils obtained with an automatic wire bonder. *Journal of Micromechanics and Microengineering* **2010**, *20*, 015021.

25. Vlnieska, V.; Voigt, A.; Wadhwa, S.; Korvink, J.; Kohl, M.; Poletkin, K. Development of Control Circuit for Inductive Levitation Micro-Actuators. *Proceedings* **2020**, *64*. doi:10.3390/IeCAT2020-08479.
26. Poletkin, K.V.; Asadollahbaik, A.; Kampmann, R.; Korvink, J.G. Levitating Micro-Actuators: A Review. *Actuators* **2018**, *7*. doi:10.3390/act7020017.
27. Poletkin, K.; Lu, Z.; Wallrabe, U.; Badilita, V. Hybrid electromagnetic and electrostatic micromachined suspension with adjustable dynamics. *Journal of Physics: Conference Series* **2015**, *660*, 012005. doi:10.1088/1742-6596/660/1/012005.
28. Poletkin, K.V. A novel hybrid Contactless Suspension with adjustable spring constant. 2017 19th International Conference on Solid-State Sensors, Actuators and Microsystems (TRANSDUCERS), 2017, pp. 934–937. doi:10.1109/TRANSDUCERS.2017.7994203.
29. Poletkin, K.V.; Shalati, R.; Korvink, J.G.; Badilita, V. Pull-in actuation in hybrid micro-machined contactless suspension. *Journal of Physics: Conference Series* **2018**, *1052*, 012035. doi:10.1088/1742-6596/1052/1/012035.
30. Poletkin, K.V. Static Pull-In Behavior of Hybrid Levitation Microactuators: Simulation, Modeling, and Experimental Study. *IEEE/ASME Transactions on Mechatronics* **2021**, *26*, 753–764. doi:10.1109/TMECH.2020.2999516.
31. Poletkin, K.V.; Korvink, J.G. Modeling a Pull-In Instability in Micro-Machined Hybrid Contactless Suspension. *Actuators* **2018**, *7*, 11. doi:10.3390/act7010011.
32. Poletkin, K. Simulation of Static Pull-in Instability of Hybrid Levitation Microactuators. ACTUATOR; International Conference and Exhibition on New Actuator Systems and Applications 2021, 2021, pp. 1–4.
33. Poletkin, K.V. *Levitation Micro-Systems: Applications to Sensors and Actuators*, 1 ed.; Springer International Publishing; p. 145. doi:10.1007/978-3-030-58908-0.